RESEARCH PAPER | Medical Science | Volume : 4 | Issue : 5 | May 2014 | ISSN - 2249-555X

Thermal Stability and Sintering Behaviour of Hydroxyapatite and Zirconia

KEYWORDS

*** Dr M. K. Hilal**

Department of Oral Maxillofacial surgery , Faculty of dentistry , Al-jabal Al-gharbi University, Gharian, Libya
* Corresponding Author

ABSTRACT *The aim of this study was to investigate the thermal stability and sintering behaviour of two hydroxyapatite and two zirconia powders, using the powder press technique. two powders of hydroxyapatite and zirconia were studied. Compacts of HAp (PB), formed by powder pressing and fired at a sintering temperature ranging from 1100 to 1500°C for 3 h for HAP and for 6 h for Zirconia, HAp(PB) could be sintered to high densities and did not dehydroxylate and/or decompose into TCP, whereas for HAp (EC) dehydroxylation and decomposition occured at lower sintering temperature than HAp (PB). A major difference was observed in the rate of densification. Densification of the ZrO_2 does not begin to take place to any great degree until sintering temperatures in excess of 1350°C are used, when employing a simple cold powder pressing (Figure 8.22). Further increasing the sintering temperature resulted in an increase in the theoretical density and linear shrinkage (Figure 8.23). The corresponding increase in biaxial flexural strength values (Figure 8.24), is thus primarily due to the densification process and secondly due to particles size distribution and transformation toughening mechanism of zirconia which was confirmed by XRD and DTA data. The BFS of ZrO_2 (U) is higher than that of ZrO_2 (M) because ZrO_2 (U) densified more than ZrO_2 (M) and that is related to the particles size distribution of ZrO_2 (U) which is smaller than ZrO_2 (M). However, statistically there is no significant difference in relation to the BFS between the two zirconia powder they behave in similar manner.*

1. INTRODUCTION

There are two major type of bioceramics, namely bioactive and bioinert ceramics.[10] The bioactive ceramics include hydroxyapatite (HAp), tricalcium phosphate (TCP), glass ionomer cement (GIC) and bioglass.[13,14,15,16,17] When these types of bioceramic are used as bone substitutes, the bone is directly chemically bonded to the material. However, these materials are mechanically weak and unsuitable for use in stress bearing areas. Alumina and zirconia are classified as bioinert ceramics which are tough and strong.[13,15,16] When such ceramics are implanted as a bone substitute they become surrounded by a fibrous tissue capsule which prevents direct bonding of the material to bone. Repeated stimulation by stress and tension at the interface leads to the growth of connective tissue, which increases the risk of loosening between the bone and ceramic implant.

ceramic has an excellent affinity to the bone because hydroxyapatite and other calcium phosphate are also the mineral components of bone.[13,14,15,16] HAp has inadequate strength and toughness to be used in stress bearing areas.[17] Two approaches have been taken to overcome this problem. Ducheyne et al.[17] used HAp as a surface layer on titanium implants, but this approach has several problems that include separation of the coating layer from the underlying bioinert matrix and the coating process can reduce the strength of the bioinert materials.[13] The second approach is to produce ceramic composites with better mechanical properties.[17,18] The hypothesis is that the even distribution of the apatite phase as islets in the strong matrix phase or visa versa will contribute to mineralization and direct bone apposition onto this type of ceramic composite.[18,19,20] This study is designed to test the validity of such an hypothesis and explores methods of production of HAp/Zirconia composites for medical and dental applications. The chemical stability during processing and characteristic properties was assessed as well as the potential interactions with the biological environment using in vitro tissue culture and in vivo animal experiments.

Zirconia is also classified as a bioinert ceramic and is noteworthy for its high strength and toughness. Zirconia has three crystal phases: monoclinic, tetragonal, and cubicThrough this phase transformation, zirconia has been shown to have a high fracture toughness. Phase transformation from tetragonal to monoclinic crystals, on the other hand, might result in a loss of strength with time.

Zirconia exhibits three well defined polymorphs, either cubic, tetragonal or monoclinic phases. It has also been shown that a high pressure orthorhombic form exists.

Monoclinic 1170 °C → Tetragonal 2370 °C → Cubic 2680 °C → Liquid

In addition, zirconia has demonstrated better wear resistance than alumina and metal alloys in some experiments and is thus considered to be a desirable and promising joint material. However, there is controversy about possible time-dependent deterioration in its mechanical properties,which make orthopaedic surgeons hesitant about using zirconia.

2. MATERIALS AND MEDODES

The materials used in this study are presented in table 1 below, where, HAp is hydroxyapatite and Y-PSZ is (3-5 mol.%Y_2O_3) yttria partially stabilized zirconia.

Table 1: The materials used in this study

Symbol	Manufacturer	Batch No.
HAp (PB)	Plasma Biotal Ltd, (Tideswell, Derbs, UK)	P120 ONS
HAp (EC)	Euro Crystals BV (Landgraaf, Holland)	91K12-1
Y-PSZ (M)	Mandoval Ltd, UK	C0523
Y-PSZ (U)	Unitec Ceramics, Stafford, UK	UCZ 373

2.1 Characterisation of the Starting Powders

The starting powders were examined using a various techniques such as wet chemical analysis for compositional information, particle size analysis for particle size and distribution and scanning electron microscopy for particles morphology.

Volume : 4 | Issue : 5 | May 2014 | ISSN - 2249-555X

a) Wet Chemical Analysis (ICP)
The wet chemical analysis as carried out by SUMAC (Sheffield, University Metallurgical Advisory Centre) employing an Inductively Coupled Plasma Spectrograph (ICP). The ICP utilises a high temperature (10,000°K) argon plasma as an excitation source.

b) Particle Size Analysis (PSA)
The particles size and their distribution of the starting powders was determined using a particle size analyser (Coulter LS 130), employing a laser diffraction method. Powders were placed in distilled water containing a few drops of defloculant (2 wt.% Sodium Hexameta Phosphate) and stirred continuously to aid dispersion for few minutes.

c) Infra-red Spectroscopy (IRS)
Infra-red spectra for both as-received and fired ground HAp powders were recorded from 200 to 4000 cm^{-1} at ambient temperature using a Perkin-Elmer 683 infra-red spectrophotometer. Samples were pelletized with KBr at a load of 10 tonnes in an evacuated die for 10 min to minimise water adsorption.

d) X-ray Diffraction (XRD)
In X-ray diffraction an X-ray beam is directed at the material which penetrates beneath the surface of the material. When the beam strikes the planes of atoms, they re-emit the radiation depending on whether the radiation being emitted is or is not in phase as shown in (Figure 8.1).

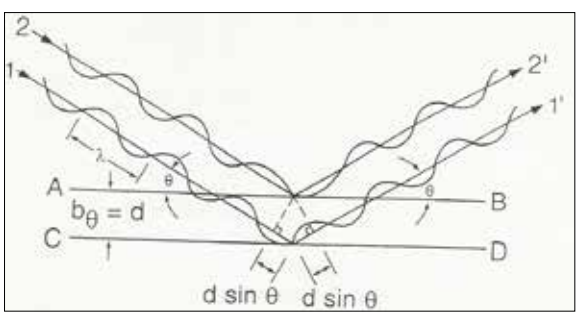

Figure 1: Diffraction of X-rays from planes of atoms.

A scan rate of 3°/min was employed over the range of 10 to 70° for all samples to be tested. 2 values of the peaks were determined from the X-ray trace and the calculated d-values compared with those listed in A.S.T.M. powder diffraction files (see appendix A).

f) Differential Thermal Analysis (DTA)
Differential thermal analysis (DTA) is a technique of recording the difference in temperature between a substance and a reference material, against either time or temperature, as two specimens are subjected to identical temperature regimes in an environment heated or cooled at a controlled rate.

g) Radioactivity Test
The radioactivity test was carried out in the Medical Physics Department, Hallamshire Hospital, University of Sheffield UK, using a Morgan Mini-monitor Scintillation (Series NO 900) with a prob type 44A (15-500 Kev ''Kilo electron volt'')

2.2 Fabrication and Characterisation of the Fired Compacts.

a) Specimen Preparation and Sintering
A single ended uniaxial steel die of 13.5 mm diameter and hand-operated hydraulic press were employed to produce green compacts of 3 mm thickness. It was found that higher compaction loads led to fracture of the compacts during pressing.

b) Density, Porosity and Shrinkage Measurements
The green and the fired compacts were weighed and their diameters and heights were measured using a micrometer (Mitutoyo, Japan). The bulk densities of the fired compacts were calculated using a geometrical method

c) Biaxial Flexural Strength Measurements (BFS)
The biaxial flexural strength for a range of firing schedules of each HAp and Y-PSZ powder was determined for 10 test-pieces. The biaxial flexural strength was calculated using the following formula:

$$\sigma_{\max.} = (\frac{P}{h^2})[0.606 \times \log e(\frac{a}{h}) + 1.13]$$

Where max. is the maximum biaxial flexural strength, P is the load at fracture, a is the radius of the knife edge support and h is the compact's thickness.

d) Microstructural Examination
The microstructure of polished sections of the fired compacts were examined using a Philips P500 SEM.

3. RESULTS

3.1.1 Hydroxyapatite
a) Characterisation of Starting Powders
The particles size distribution of the two HAp powders is presented in Figure 8.2 and clearly shows a difference in the particle size distribution of the two powders. The PB powder has a considerably smaller particle size distribution than the EC powder, with a mean particle size of 5.12 m and 15.06 m respectively. This appears to concur with the SEM observation that the PB is a loosely packed and the EC a tightly packed agglomerated structure as shown in Figure 8.3.

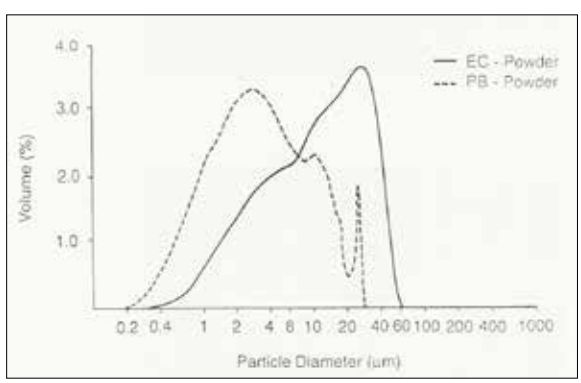

Figure 2: Particles size distribution for HAp powders.

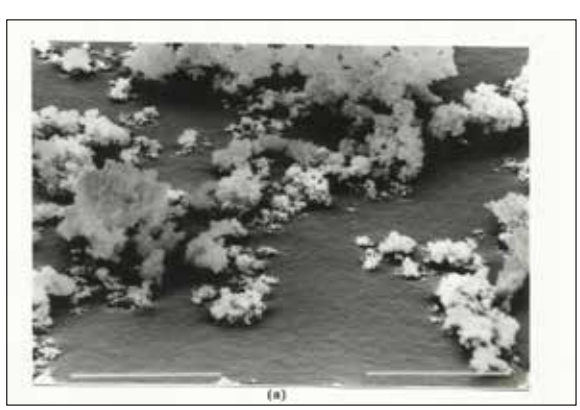

Volume : 4 | Issue : 5 | May 2014 | ISSN - 2249-555X

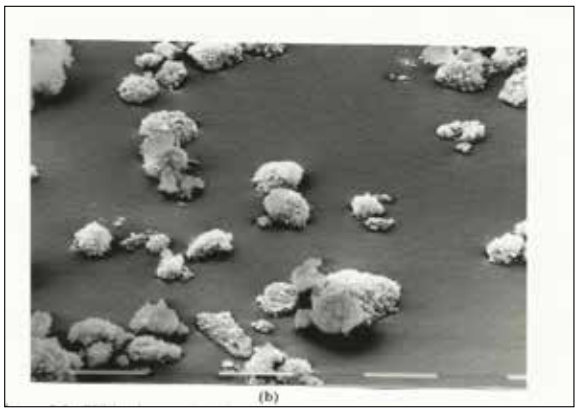

Figure.3: SEM micrographs of the particle morphologies of HAp powders, showing the loosely packed particles of PB (a) and closely packed particles of EC (b). original magnification. 2500 (Scale bar = 10m)

The wet chemical analysis shows that, the Ca/P ratio of EC powder was 1.69 0.2 and for PB powder was 1.67 0.2 which is close to the Ca/P ratio for stoichiometric HAp.192,197,198,199

The infra-red absorption spectra of powder EC and PB are shown in Figure 8.4 a and b respectively, and are similar to those presented by other investigators.228,229

b) Characteristics of the Fired Powders

IR spectra over a restricted wave number range of 200-800 cm^{-1} are presented for the PB and EC powders in Figure 8.5 for the range of firing temperatures investigated. It can be seen that both materials lose their hydroxyl groups as indicated by the gradual disappearance of the OH peaks at 630 cm^{-1}. The results show that EC begins to dehydroxylate at 1150°C, whereas for PB this occurs at the slightly higher temperature of 1200°C.

The XRD data for powder EC in the as-received state and after firing at 1100°C, 1200°C and 1400°C are presented in Figure 8.6. This powder shows no difference to XRD data obtained for the as-received powder PB presented in Figure 8.7 and compared to data previously reported.187 The XRD traces of the fired materials had sharper peaks. EC was stable up to 1200°C and started to decompose at a temperature in excess 1200°C when peaks attributable to -TCP began to appear as identified in Figure 8.6. In contrast, PB is more stable and only at temperatures of 1250°C and higher do -TCP peaks begin to appear (Figure 8.7). For both materials, when fired at a sintering temperature of more than 1350°C, the -TCP disappeared and -TCP formed instead.

The DTA curves for EC and PB powders are shown in Figure 8.8. An endothermic peak was observed in the range from 200 to 400°C, which is probably due to water loss. An endothermic peak was observed at 1150-1350°C for HAp (EC) and 1200-1350°C for HAp (PB) which is due to transformation of HAp to -TCP. Another endothermic peak for both powder was also observed at about 1450°C which is due to the complete transformation of -TCP into -TCP as confirmed by XRD results.

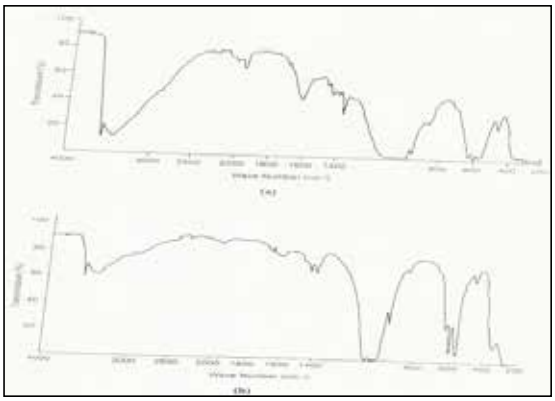

Figure.4: Infrared (IRS) spectrum of hydroxyapatite as-received (a) EC and (b) PB

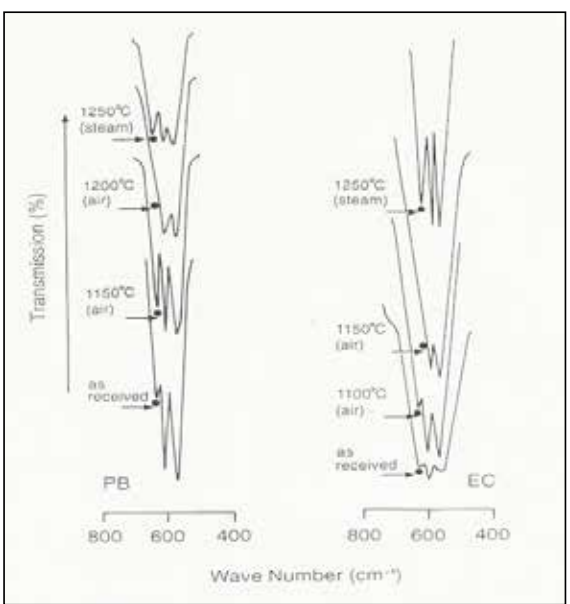

Figure5: IRS spectra of PB and EC powders after having been fired in air and steam for 3 h at the temperatures indicated. Note the retention of the 630 cm^{-1} peak when fired in steam at 1250°C.

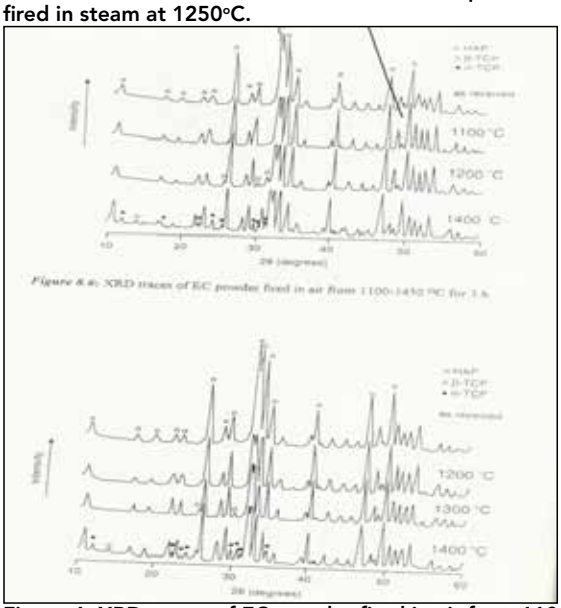

Figure 6: XRD traces of EC powder fired in air from 1100-1450°C for 3 h.

Volume : 4 | Issue : 5 | May 2014 | ISSN - 2249-555X

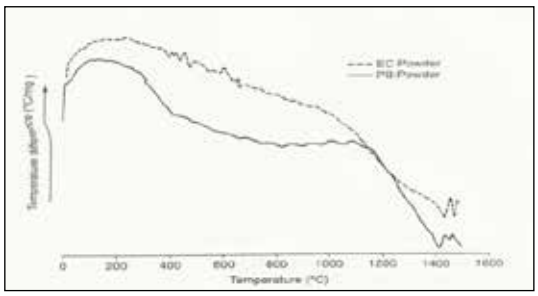

Figure 8: DTA analyses for both hydroxyapatite powders fired in air atmosphere from 0-1500 °C.

c) Sintering Behaviour and Biaxial Flexural Strength

The % of the theoretical density, true porosity and linear firing shrinkage were plotted as a function of sintering temperature (Figures. 8.9, 8.10 and 8.11). Both materials became more dense when the sintering temperature increased from 1100°C to 1450°C. The linear shrinkage increased, and the true porosity decreased as can be seen in the SEM migrograph (Figures 8.12 and 8.13). Scanning electron micrographs of a thermally etched surface of compacts PB and EC sintered in air at 1250 °C for 3 h are shown in Figure 8.14, revealing a close similarity in the grain structure and in the average grain size (PB = 5.5 and EC = 6.2 m) of both forms of HAp.

The biaxial flexural strength data show that their biaxial flexural strength increased with increasing the sintering temperature up to 1300°C (Figure 8.15). The maximum biaxial flexural strength values of 93 MPa and 100 MPa for PB and EC materials respectively were achieved. Above 1300°C, the biaxial flexural strength of both materials reduced rapidly, due to decomposition of HAp into TCP, which causes cracking on the surface of compacts as shown in Figure 8.16, and result in a flaw initiating fracture.

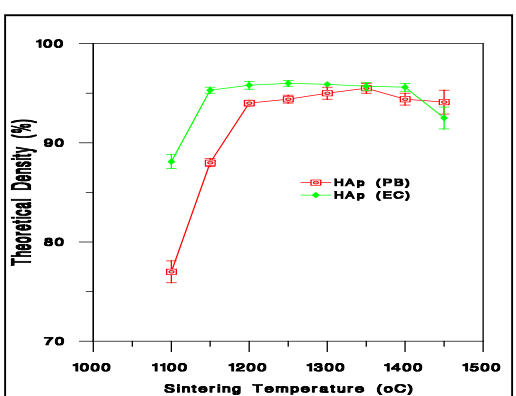

Figure 8 9: The effect of sintering temperature on the % theoretical density of HAp (PB) and HAp (EC) compacts, fired for 3 h in an air atmosphere.

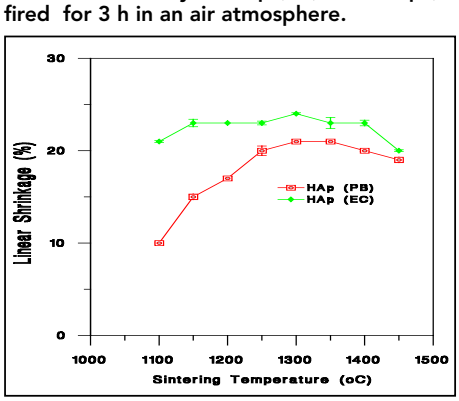

Figure 10: The effect of sintering temperature on the % linear shrinkage of HAp (PB) and HAp (EC) compacts, fired for 3 h in an air atmosphere.

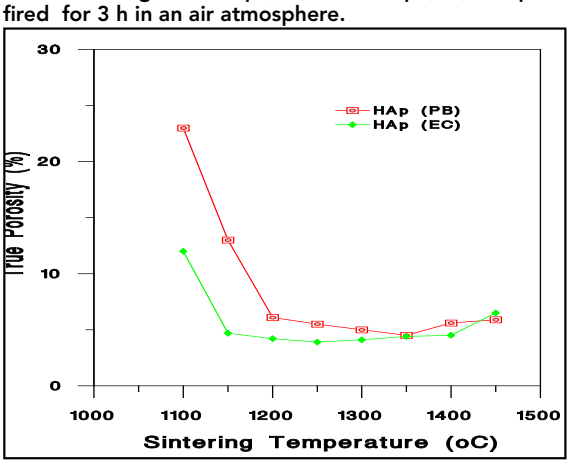

Figure 11: The effect of sintering temperature on the % true porosity of HAp (PB) and HAp (EC) compacts, fired for 3 h in an air atmosphere.

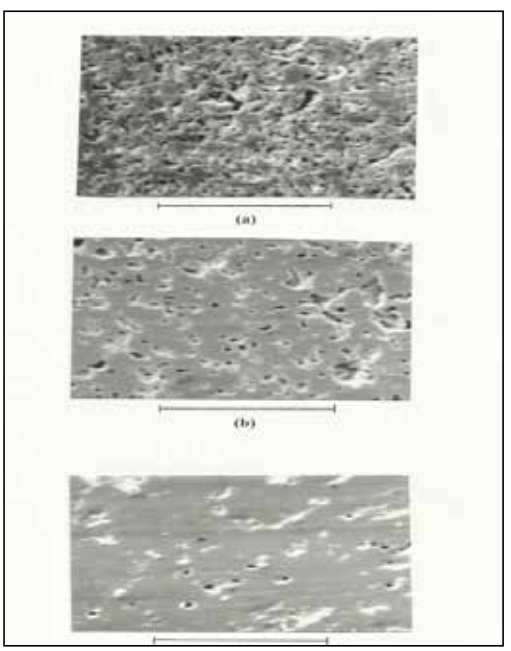

Figure.12: SEM micrographs of polished section of compacts of PB sintered for 3 h. at a sintering temperature of (a) 1100°C (b) 1200°C (c) 1300°C. Original mag. 2500 (Scale bar = 20 m)

Figure 13: SEM micrographs of polished section of compacts of EC sintered for 3 h. at a sintering temperature of (a) 1100 oC (b) 1200 oC (c) 1300 oC. Original mag. 2500 (Scale bar = 20 m)

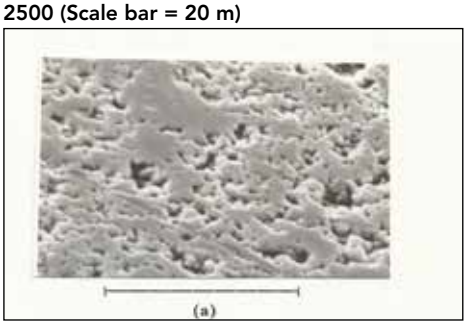

Volume : 4 | Issue : 5 | May 2014 | ISSN - 2249-555X

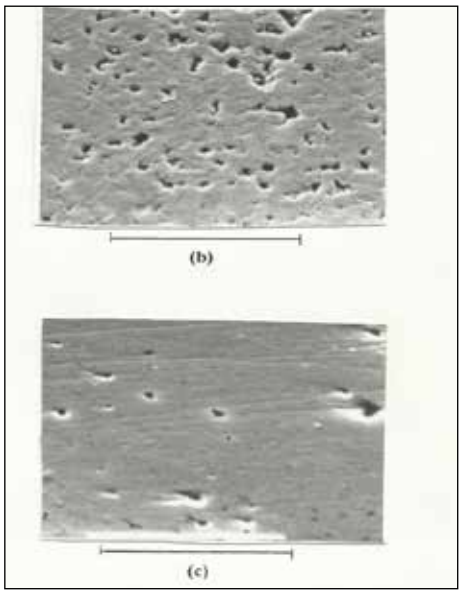

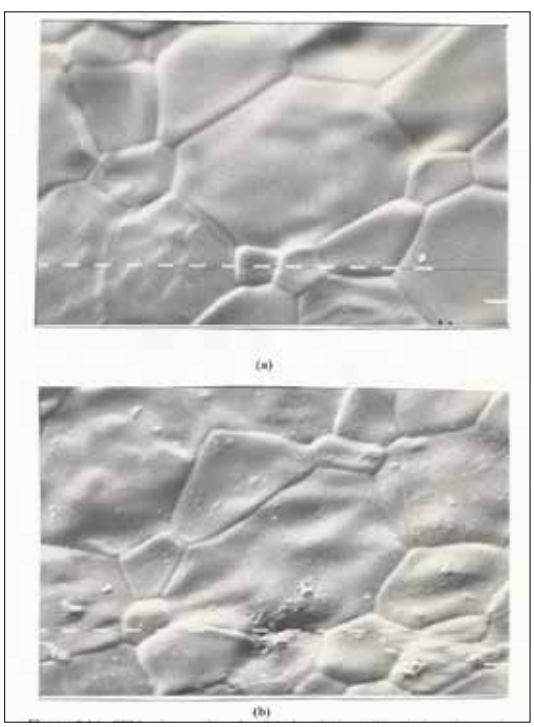

Figure 14: SEM micrographs of polished and thermally-etched surfaces of compacts of (a) PB and (b) EC, fired at 1250 °C for 3 h. Original mag. 2500 (Scale bar = 1 m).

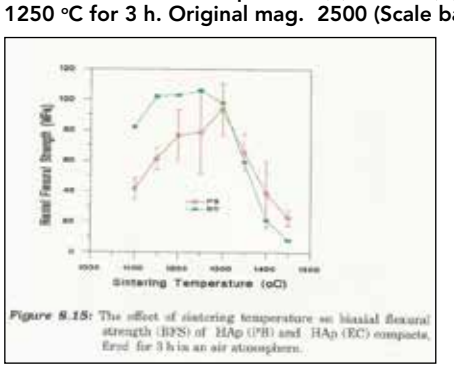

Figure 8.15: The effect of sintering temperature on biaxial flexural strength (BFS) of HAp (PB) and HAp (EC) compacts, fired for 3 h in an air atmosphere.

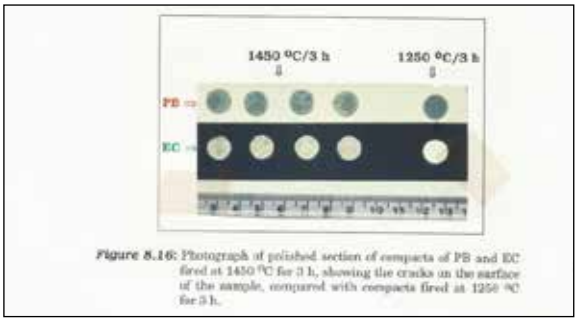

Figure 8.16: Photograph of polished section of compacts of PB and EC fired at 1450 °C for 3 h, showing the cracks on the surface of the sample, compared with compacts fired at 1250 °C for 3 h.

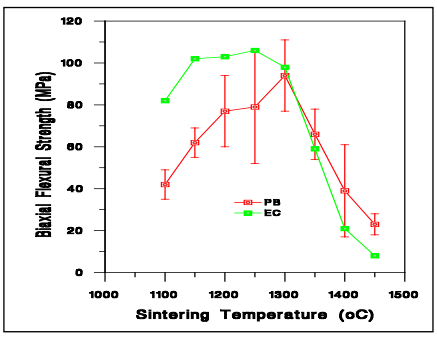

Figure 8.15: The effect of sintering temperature on biaxial flexural strength (BFS) of HAp (PB) and HAp (EC) compacts, fired for 3 h in an air atmosphere.

3.2 Zirconia

a)Characteristics of Starting Powders

Table 8.2. shows the wet chemical analysis (ICP) for the main compositional elements of both ziconia powders.

Table.2: The wet chemical analysis of zirconia powders.

Element	Amount	
	Y-PSZ (U)	Y-PSZ (M)
Zr	50.4%	53.3%
Y	2.96%	3.20%
Al	0.10%	0.11%
Ca	0.03%	0.02%
Si	0.20%	0.15%

PSA data are presented in Figure 8.17. The mean particle size of Y-PSZ (U) was 0.5m and of Y-PSZ (M) was 1.6 m. Both powders were agglomerated as shown in the SEM micrographs of zirconia (Figures 8.18). The XRD data for both ZrO_2 powders (Figures.19 and 20) shows that their consist of a mixture of tetragonal (t), monoclinic (m) and cubic (c) phases.

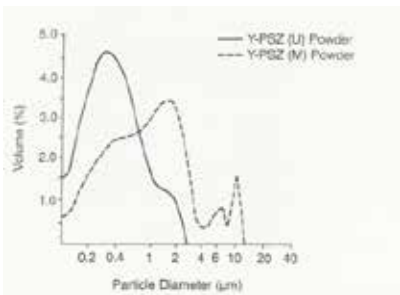

Figure 8.17: Particles size distribution for Y-PSZ powders.

Volume : 4 | Issue : 5 | May 2014 | ISSN - 2249-555X

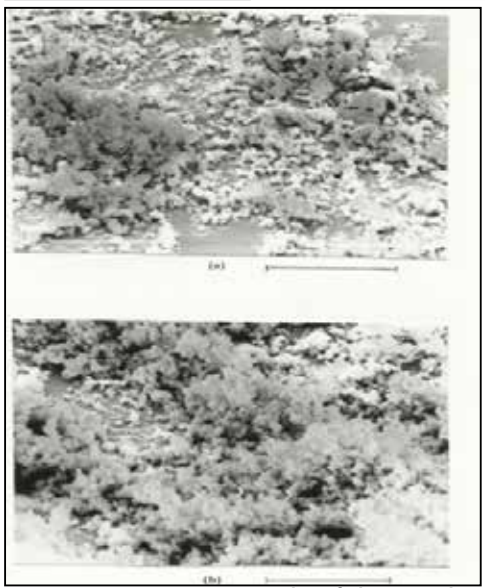

Figure 8.18: SEM micrographs of the particle morphologies of zirconia powders, showing the loosely packed particles of (a) Y-PSZ (U) and (b) Y-PSZ (M). Original magnification. 2500 (Scale bar = 10m).

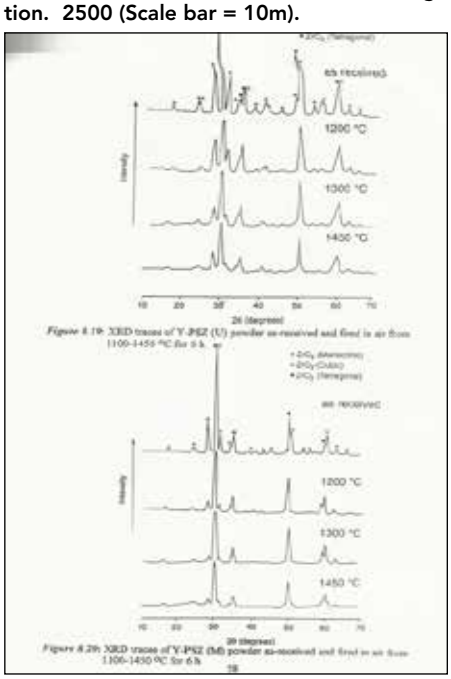

b) Characteristics of the Fired Powders

XRD data for the fired compacts of Y-PSZ (U) and Y-PSZ (M) are also shown in Figures 8.19 and 8.20 respectively, which show that there is a reduction in the peak of the monoclinic phase with increasing firing temperature.

The DTA curves for Y-PSZ (U) and Y-PSZ (M) powders are shown in Figure 8.21. These curves show an endothermic peak at about 200-400°C, may be due to water loss. At about 1170-1200°C there is an endothermic peak which could be due to the transformation of monoclinic to the tetragonal phase.

c) Sintering Behaviour and Biaxial Flexural Strength (BFS)

The theoretical density, linear firing shrinkage and the biaxial flexural strength values were plotted against sintering temperature, as shown in Figures 8.22, 8.23 and 8.24 respectively. These were found to increase with increasing sintering temperature, whereas true porosity found to decrease as seen in the SEM migrographs (Figures 8.25 and 8.26).

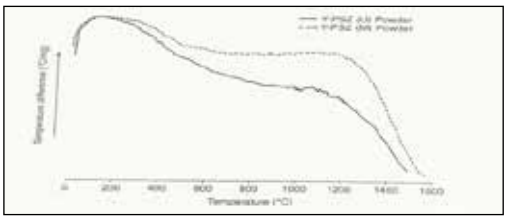

Figure 8.21: DTA analyses for both zirconia powders fired in air atmosphere from 0-1500 °C.

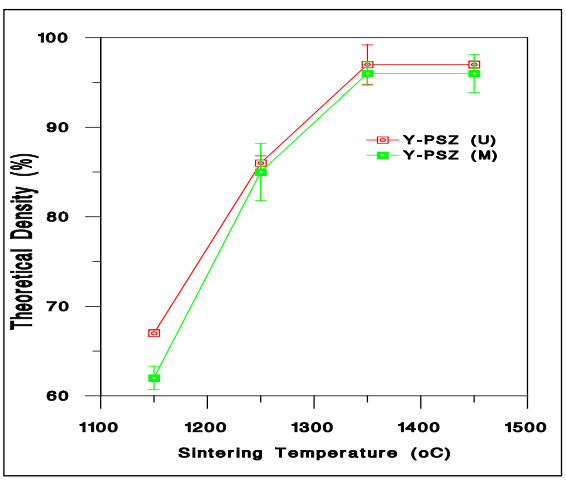

Figure 8.22: The effect of sintering temperature on the % theoretical density of Y-PSZ (U) and Y-PSZ (M) compacts, fired for 6 h an in air atmosphere.

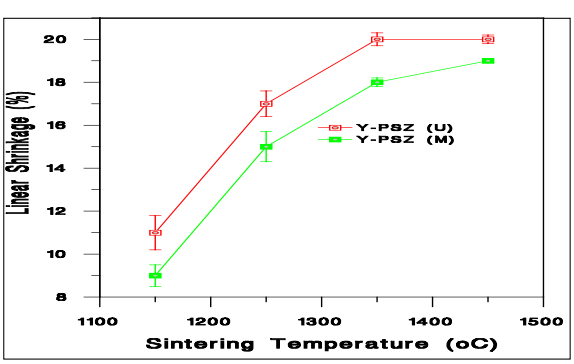

Figure 8.23: The effect of sintering temperature on the % linear shrinkage of Y-PSZ (U) and Y-PSZ (M) compacts, fired for 6 h in an air atmosphere.

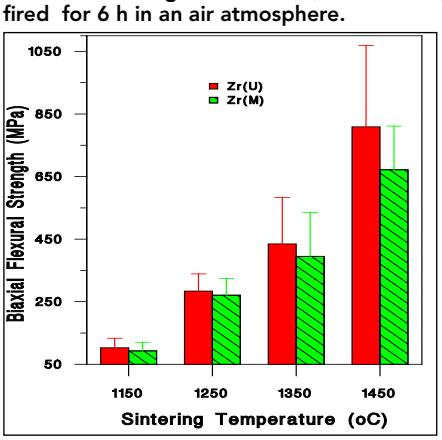

Volume : 4 | Issue : 5 | May 2014 | ISSN - 2249-555X

Figure 8.24: The effect of sintering temperature on the biaxial flexural strength of Y-PSZ (U) and Y-PSZ (M) compacts, fired for 6 h in an air atmosphere.

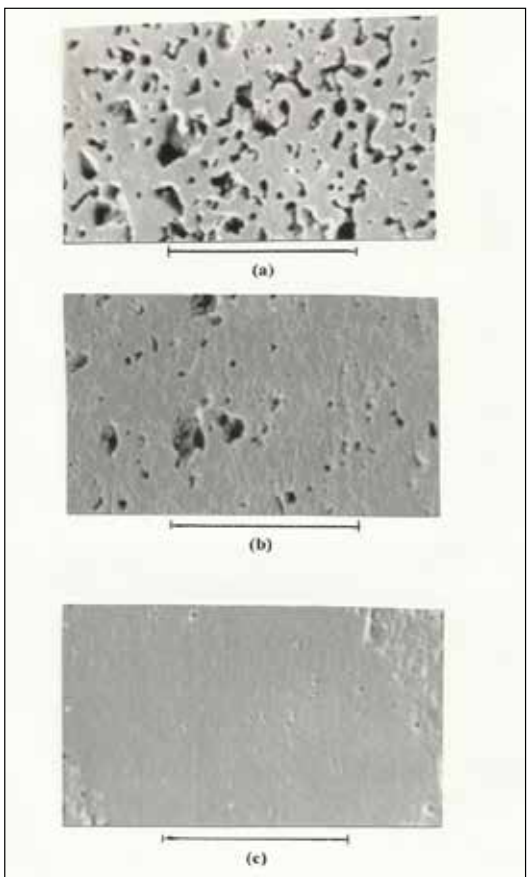

Figure 8.25: SEM micrographs of polished section of compacts of Y-PSZ (U) sintered in air for 6 h at a sintering temperature of (a) 1200°C (b) 1300°C (c) 1450°C. Original mag. 2500 (Scale bar = 20 m)

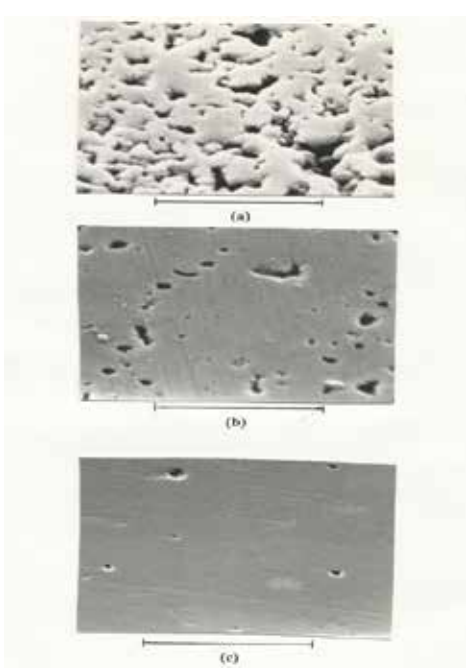

Figure 8.25: SEM micrographs of polished section of compacts of Y-PSZ (M) sintered in air for 6 h at a sintering temperature of (a) 1200°C (b) 1300°C (c) 1450°C. Original mag. 2500 (Scale bar = 20 m)

4.DISCUSSIONS

4.1 Hydroxyapatite

In this phase of the study, the thermal stability, sintering behaviours and mechanical properties of the two hydroxyapatite powders were investigated.

IR spectroscopy was employed to investigate whether the dehydroxylation process occurred during firing in either air or a steam atmosphere. The results show that EC begins to dehydroxylate at 1150°C, whereas for PB this occurs at the slightly higher temperature of 1200°C. This observation confirms that of other workers where temperatures for the onset of dehydroxylation have been found to vary depending on the source powder

The XRD data for both HAp powders in the as-received state appear to be identical and consist of high purity and highly crystalline HAp (Figures 8.6 and 8.7). They show no discernible difference to data obtained from A.S.T.M powder diffraction file (Appendix A) For both materials, when fired at a sintering temperature of more than 1350°C, the -TCP disappeared and -TCP formed instead, which confirms similar findings by other investigator. The better stability of PB at higher sintering temperature may related to the greater purity of this HAp powder, as can be seen from wet chemical analysis (ICP).

The DTA data for EC and PB powders (Figure 8.8) show an endotherm in the range of 200-400°C, which is due to water loss. Another endothermic peak was observed at 1350°C which is due to decomposition of hydroxyapatite to TCP and confirmed by XRD to be a mixture of -TCP and -TCP. Beyond 1400°C an endothermic peak was also observed which is due to the complete transformation of -TCP to -TCP as confirmed by XRD and in agreement with other investigators results.

Scanning electron micrographs of the thermally etched surfaces (Figure 8.14), revealed a close similarity in the grain structure of both forms of HAp. As might be expected from the increased density with higher firing temperature, the biaxial flexural strength increased with increasing sintering temperature up to 1250°C for (EC) and 1300°C for (PB). EC reached its maximum BFS at 1150°C whereas PB did not achieve its maximum until 1300°C, (i.e. just as is reaches its decomposition temperature). This difference is due to the rapid densification of EC compared with PB virtue of its slightly higher density.

4.2 Zirconia

The XRD data for both ZrO_2 powders (Figures 8.19 and 8.20) show the three phases for zirconia, and since monoclinic zirconia has peaks at about the same positions as its cubic form, a definite distinction of the second phase was difficult.

XRD data for both fired powder, showed that there was a sharp peak (the relative intensity of the peak increased) at 2 = 30.6° for the tetragonal and/or cubic phase, and a reduction in the peaks of monoclinic phase (the relative intensity of the peak decreased gradually) with increasing the firing temperature, at 2 = 17.6, 24.1, 28.2 and 37°. This suggests that there is a transformation of monoclinic phases into tetragonal phases. These results an in accordance with most of the reported studies.

Lange,[24] Chaim,[23] Rhule,[22] proposed that materials containing the higher Al_2O_3 and SiO_2 contents would form the glassy phase more readily and that this glassy phase would facilitate rapid liquid phase sintering at lower temperatures. However at higher temperatures the glassy phase would be dissolved in the t-ZrO_2 grains and slower solid state sintering would become the predominant mechanism.

Volume : 4 | Issue : 5 | May 2014 | ISSN - 2249-555X

The BFS of Y-PSZ (U) is higher than that of Y-PSZ (M) because Y-PSZ (U) densified more than Y-PSZ (M) and because the particles size distribution of Y-PSZ (U) is finer than that for Y-PSZ (M). There is a higher driving force and higher rate of sintering with finer particles, which have a higher specific surface area than coarser particles.

Scanning electron micrograph (Figures 8.25 and 8.26) show the effect of sintering temperature on the microstructure of sintered zirconia compacts.

The result of the radioactivity test indicated that none of the materials used in this study were radioactive, including zirconia.

5. Conclusions

1. Powder PB is more resistant to dehydroxylation and decomposition than EC.

2. Powder EC shows a more rapid densification than powder PB, especially at sintering temperatures of less than 1200°C.

3. Dehydroxylation did not effect the biaxial flexural strength of either hydroxyapatites.

4. The transformation of HAp to -TCP causes a substantial loss of biaxial flexural strength.

5. The physical and mechanical properties of the stabilised zirconias are dependent on not only microstructure, but also particles size, chemical composition and sintering stability of the powders.

6. There is large difference in the two zirconia powders in terms of powder particles size, with Y-PSZ (U) been smaller than Y-PSZ (M). These differences lead to different sintering behaviours in the two powders and hence the mechanical properties.

REFERENCE

1. Williams D. F., Black, J. and Doherty P. J., Second Consensus Conference on Definitions in Biomaterials, In: Biomaterial-tissue interfaces; Advances in Biomaterials vol. , Doherty et al. (eds), Elsevier Science Publishers, London, 10: 525-533, 1992. | | 2. Williams, D. F. Review Biodegradation of surgical polymers. J. Mat. Sci. 17: 1233-1246, 1982 | | 3. Branemark P. I., Osseointegration and its experimental background. J. Prosthet. Dent. 50: 399-412, 1983. | | 4. Davis, J. E. and Matsuda, T. Extracellular matrix production by osteoblasts on bioactive substrata in vitro. Scanning Microscopy 2(3): 1445-1452, 1988. | | 5. Le Geros, R. Z., Orly, I. Gegoire, M. and Deculsi, G. Substrate surface dissolution and interfacial biological mineralisation. In: the bone biomaterial interface. Davies, J. E. (ed.). Univ. Toronto Press, 76-88, 1991. | | 6. Lemons, J.E., Natiella, J. Biomaterials, biocompatibility and pre-implant considerations. Dent. Clin. N. Am. 30: 3-23, 1986. | | 7. Jarcho, M. Biomaterial aspects of calcium phosphates properties and applications, Dent. Clin. N. Am. 30: 25-47, 1986. | | 8. Meffert, R. M., Langer, B. and Fritz, M. E., Dental implants: a review. J. Periodontol. 63: 859-870, 1992. | | 9. Young, F. A., Future directions in dental implants research. J. Dent. Educ. 52: 770-774, 1988. | | 10. Kent, J.N. and Bokros, J.C., Pyrolytic carbon and carbon-caoted metallic dental implants. Dent. Clin. N. Am. 24: 465-504, 1980. | | 11. Schnitman, P.A. and Shulman, L. B., Vitreous carbon implants. Dent. Clin. N. Am. 3: 441-463, 1980. | | 12. Mah, C. The evaluation of implants over the last fifty years. Aust. Prosthodont. J. 4: 47-52, 1990. | | 13. Suda, A., Sato, T., Takagi, M., Osanai, T. and Suzuki O., Biocompatibility of zirconia dispersed hydroxyapatite ceramics, J. Jpn. Orthop. Assoc. 64: 249-259, 1990. | | 14. Hench, L. L. and Paschall, H. A., Direct bond of bioactive glass-ceramic materials to bone and muscle, J. Biomed. Mater. Res. 4: 25-43, 1973 | | 15. Hench, L. L. and Paschall, H. A., Histochemical responses at a biomaterial's interface, J. Biomed. Mater. Res. Symp. 5: 49-64, 1974. | | 16. Gross, U. M., Brandes, J., Strunz, V., Bab, I. and Sela, J., The ultrastructure of the interface between a glass ceramic and bone, J. Biomed. Mater. Res. 15: 291-305, 1981. | | 17. Ducheyne, P., Hench, L.L., Kagan, A., Martens, M., Burssens, A., and Mulier, J.C. Effect of hydroxyapatite impregnation on skeletal bonding of porous coated implants, J. Biomed. Mater. Res. 14: 225-337, 1980. | | 18. Wu, J-M. and Jeh, T-S. Sintering of hydroxyapatite-zirconia composite materials., J. Mater. Sci: Mater. Med. 23: 3771- 3777, 1988. | | 19. Li, J., Hermansson, L. and Soremark, R., High-strength biofunctional zirconia: mechanical properties and static fatigue behaviour of zirconia-apatite composites, J Mater. Sci: Mater. Med. 4: 50-54, 1993. | | 20. Takagi, M., Mochida, M., Uchida, N., Saito, K. and Uematsu, K. Filter cake forming and hot isostatic pressing for TZP-dispersed hydroxyapatite composite, J. Mater. Sci.: Mater. Med. 3: 199-203, 1992. | | 21. Brook, I. Evaluation of glass-ionomer cements for use as bone substitutes with reference to their value for treatment of atrophic alveolar bone, Ph.D Thesis University of Sheffield, UK. 1993. | | 22. Rhule. General anatomy and histology of bone. In: Biochemistry and physiology of bone Bourne,G.M. (ed). Academic Press, New York, 1965. | | 23. Chaim A. and Krajewski. Physical properties and physiology of bone. Pub Chapman and Hall, London, 16-39, 1992. | | 24. Lange, S. Cheug and Michael, H. Growth of osteoblasts on porous calcium phosphate ceramics: an in vivo model for biocompatibility study. J. Biomaterials. 10: 63-67. 1989. |